

MONASH University

Understanding texture effects on deformation mechanisms in Zircaloy-4

Ethan Sprague

PhD Confirmation Milestone Report

Supervisors:

Prof. Michael Preuss

Dr. Fatemeh Azhari

Dr. Dylan Agius

Abstract

Zircaloy-4 and other hexagonal phase alloys develop strong and unavoidable crystallographic textures during conventional processing. The effects of this texture are difficult to decouple from the underlying deformation mechanisms. The texture results in highly anisotropic response, where loading along different directions results in vastly different yield behaviours. Powder metallurgy and hot isostatic pressing (HIP) were used to produce hexagonal metals that have a fully random crystallographic texture. The HIP process requires a long dwell at high temperature below the beta-transus, which leads to abnormal grain growth in some circumstances, however a successful HIP process was eventually determined. Calculated Kearns factors and the disorientation distribution confirm that a random texture was obtained. Statistical geometric alignment between neighbour grains revealed a measurable difference between the strongly textured material and the HIPed material. The presence of strong texture results in a statistical peak in well-aligned grains, which was not present for the random texture material, indicating a much higher average constraint by neighbouring grains. Proposed future work for this project includes fitting crystal plasticity models to the random texture material and in-situ mechanical testing with high resolution digital image correlation to track strain propagation within the microstructure.

Contents

Abstract	i
1 Introduction	1
2 Literature review	3
2.1 Deformation modes	3
2.1.1 Slip	3
2.1.2 Twinning	5
2.2 Texture development	6
2.3 Slip transfer	6
3 Research aims	9
4 Methodology	11
4.1 Hot Isostatic Press (HIP)	11
4.2 Optical microscopy	12
4.3 Electron Backscatter Diffraction (EBSD)	13
4.4 Mechanical testing	13
4.5 Crystal plasticity modelling	14
5 Research completed to date	15
5.1 CP-Ti plate	15
5.2 HIP #1: Abnormal grain growth	18
5.3 HIP #2: Success	19
5.3.1 Geometric compatibility	21
6 Proposed research	23
6.1 Mechanical testing of HIPed material	23
6.2 HR-DIC in-situ testing	23
6.3 Rolling HIPed material	23
6.4 Crystal plasticity modelling	24
7 Research communication	25
Bibliography	26

Chapter 1

Introduction

The cladding for the nuclear fuel of pressurised water reactors is a critical component for which reliable integrity evaluations must be made over the entire fuel cycle, from service to waste storage. Zirconium alloys are selected for the cladding material because of their low neutron absorption, good corrosion resistance and suitable mechanical properties. It is crucial that the mechanical behaviour of these alloys is well understood, and accurate models are necessary for safety assessments. Increasingly, advanced safety systems use a 'digital twin' model of the entire reactor which must accurately predict the mechanical response of the cladding material during simulated emergencies.

Zirconium alloys used for cladding have a hexagonal close packed (HCP) crystal structure. These alloys always develop a strong crystallographic texture during conventional processing such as rolling and pilgering. This crystallographic texture has a significant impact on the mechanical behaviour, resulting in a large anisotropy and directional dependence. Furthermore, the texture impacts other properties such as the formation sites for hydrides, which preferentially grow along specific crystallographic planes. Finally, polycrystalline deformation requires each grain to accommodate the deformation of its neighbour grains, even when there is a mismatch in the single crystal properties due differences in orientation. These neighbour interactions must be taken into account during both in-service and storage conditions, where thermal cycling and variations in pressure can lead to heterogeneous deformation.

The seemingly unavoidable crystallographic texture which emerges from processing dominates samples that are used to study the behaviour of these alloys. Since texture has such a large effect, it is possible that underlying behaviours are being obscured by texture effects. Material modelling should be able to accurately predict the mechanical performance of these alloys for any given texture, however, these models have only ever been extensively tested against data from strongly textured material.

This project uses powder metallurgy techniques, namely hot isostatic pressing (HIP) to create HCP material with a truly random texture by eliminating all sources of directional stress. Studying this material alongside its conventionally processed equivalent enables a far more robust approach to optimising existing material models, with the additional constraint of a randomly textured material.

This work is directed at understanding zircaloy-4, but the results will have broader impact more generally on similar hexagonal metals such as α -titanium alloys. The new in-situ testing capabilities at Monash Centre for Electron Microscopy provide the opportunity to understand the complex and asymmetric deformation within these hexagonal polycrystalline materials, allowing for a deeper understanding on fundamental deformation of an entire class of alloys. Finally, this project opens the pathway for future study on other texture-related phenomenon such as the effect of hydrides in texture-free material.

Chapter 2

Literature review

2.1 Deformation modes

HCP metals, such as α titanium and zirconium, exhibit complex plastic deformation behaviour which is a direct consequence of the intrinsic anisotropy of their low-symmetry crystal structure. In contrast to FCC metals which have 12 independent and evenly distributed slip systems which can facilitate homogenous deformation for any arbitrary shear, HCP metals rely on a more restricted set of slip systems with widely varying critical resolved shear stresses (CRSS). Many of the HCP slip systems are not independent, meaning the shear strain that they provide can be equivalently facilitated by a linear combination of other slip systems. The Von-Mises criterion states that 5 independent slip systems are required to facilitate homogenous arbitrary deformation. In order to satisfy this condition in HCP, more complex modes such as difficult pyramidal $\langle c+a \rangle$ or deformation twinning must be activated.

2.1.1 Slip

The most favourable slip occurs along crystal planes with the highest atomic packing density. For a HCP structure with an ideal c/a ratio, this would be the basal $(0\ 0\ 0\ 2)$ plane, however in both titanium and zirconium the c/a ratio is less than the ideal value of 1.633, being 1.587 and 1.593 respectively [2, 3]. This compacted HCP structure results in the highest atomic density on the prismatic planes $\{1\ 0\ \bar{1}\ 0\}$, followed closely by the basal plane $(0\ 0\ 0\ 2)$. The slip direction on both of these planes occurs along the $\langle a \rangle$ direction $\langle 1\ 1\ \bar{2}\ 0 \rangle$. Because the Burgers vector of both of these slip families is shared, they cannot provide any shear strain that has a $\langle c \rangle$ -axis component. If one considers a loading along the $\langle c \rangle$ -axis, the Schmid factor for both basal and prismatic slip would be

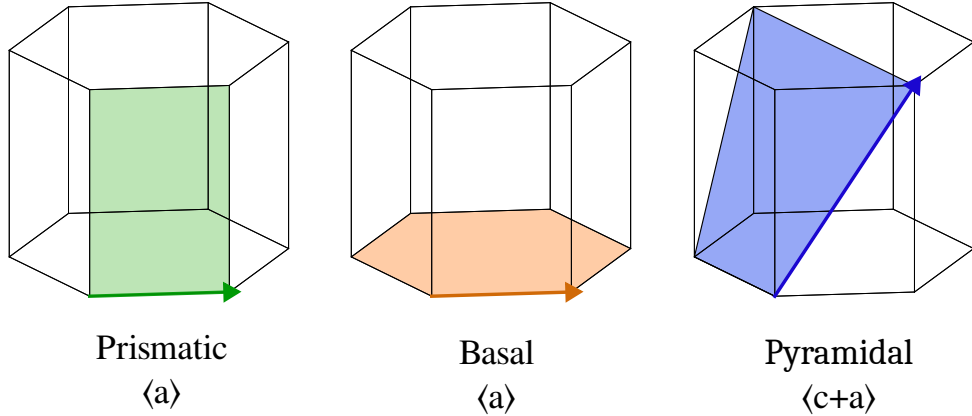


FIGURE 2.1: Dominant slip modes in hcp metals.

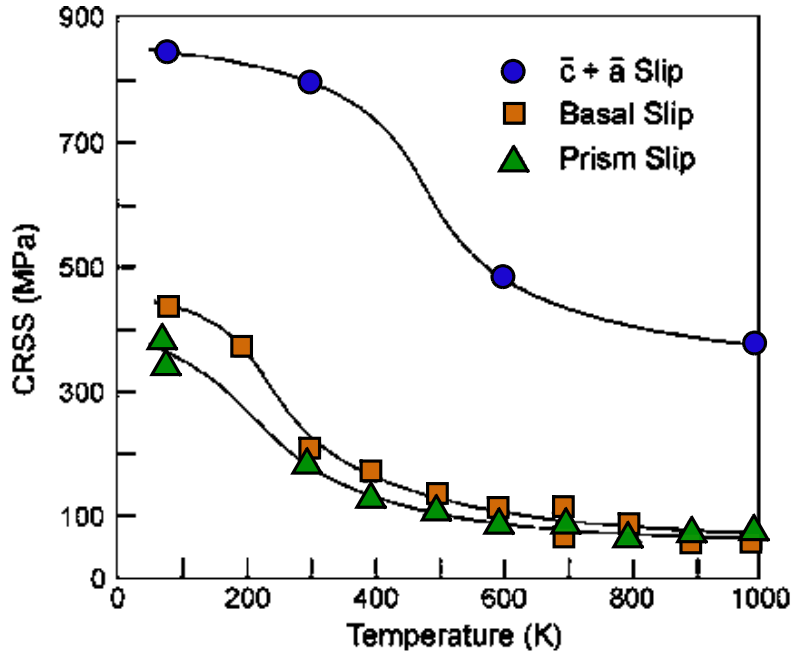


FIGURE 2.2: Critical resolved shear stresses in Ti-6.6Al single crystal [1].

zero, meaning plastic deformation must come from another slip mode from a plane that necessarily has a lower atomic density. The slip mode that activates in this case is the pyramidal $\langle c+a \rangle$, on the $\{10\bar{1}1\}$ plane along the $\langle 11\bar{2}3 \rangle$ direction which is the sum of the $\langle c \rangle$ and $\langle a \rangle$ basis vectors. Figure 2.2 compares the CRSS values for these three major

slip modes as a function of temperature in a Ti-6.6Al single crystal. The vast difference in CRSS between the $\langle a \rangle$ and $\langle c+a \rangle$ slip modes results in the heavily anisotropic plastic behaviour of HCP metals. The crystal orientation of a grain therefore becomes one of the most important factors determining how it will deform, since this will dictate which of the slip modes will be active and what the resolved shear stress will be [3–5].

2.1.2 Twinning

Deformation twinning offers an alternative way for the crystal structure to accommodate $\langle c \rangle$ -axis strain and is often the favourable mode due to the high CRSS of pyramidal $\langle c+a \rangle$ slip. The available twinning modes are listed in Table 2.1, which are classified into tensile and compression type twins based on the $\langle c \rangle$ component of the shear. Twinning is a coordinated reorientation of the lattice and has a distinct orientation relationship with the parent crystal, which can be defined in terms of an angle-axis representation, also listed in Table 2.1. All of these twin modes result in a tilting of the $\langle c \rangle$ -axis, this means that the resulting crystal within the twin volume will be quite distinct from its parent material in terms of plastic response. For example, for loading along the $\langle c \rangle$ -axis a grain will initially be quite hard. If the Type I tensile twin activates, the resulting region will have its $\langle c \rangle$ -axis tilted by 85° , resulting in quite a soft orientation that is well aligned for prismatic slip.

Twinning mode	K_1	Angle – axis	ε
Tensile Type I	$\{10\bar{1}2\}$	$85^\circ\langle11\bar{2}0\rangle$	0.171
Tensile Type II	$\{11\bar{2}1\}$	$35^\circ\langle1\bar{1}00\rangle$	0.629
Compression Type I	$\{11\bar{2}2\}$	$65^\circ\langle\bar{1}100\rangle$	0.221
Compression Type II	$\{10\bar{1}1\}$	$54^\circ\langle12\bar{1}0\rangle$	0.101

TABLE 2.1: Twinning systems with twin plane, axis-angle representation, and twinning shear ε . [6]

Unlike slip, deformation twinning has limited activity and eventually becomes exhausted. In HCP metals, twinning occurs in the early stages of plasticity where it plays a large role in accommodating $\langle c \rangle$ -axis strain in grains that are poorly aligned for prismatic slip [6]. After twin nucleation and growth, eventually the twins consume the majority of their initial grains and subsequent plasticity can continue through dislocation slip.

Deformation twinning adds to the complexity of HCP metals since twin boundaries act as barriers to dislocation motion and secondary twins can form within the primary twin volume [7]. An accurate description of the deformation behaviour of HCP metals must take all of this into account.

2.2 Texture development

Conventional processing of HCP alloys always produces strong crystallographic texture. In the case of α -titanium and zirconium which have a similar c/a ratio, the particular texture that develops during cold rolling is a basal texture with a split toward the transverse direction of $\pm 25 - 35^\circ$ [8]. Texture develops during cold working because of the significant crystallographic reorientation that is associated with deformation twinning. The roller imposes a compressive stress normal to the plane of the plate, but due to the Poisson effect there is a tensile stress in the plane of the plate. Both compressive (Type I) and tensile (Type I and II) twins have been observed to activate under cold rolling conditions [9]. The twinning activity during the early stages of plasticity cause a significant initial texture change, and then subsequent plastic slip may cause further crystallographic reorientation [10]. Unlike twinning which causes an immediate reorientation, slip results in a gradual rotation. Prismatic slip, which is the most active slip mode, results in a rotation about the $\langle c \rangle$ -axis, while basal and pyramidal $\langle c+a \rangle$ cause the $\langle c \rangle$ -axis to tilt.

The final texture that is present after cold rolling is inherited by the recrystallised microstructure, possibly due to preferential nucleation within the twinned regions [11]. The exact processing route and parameters effect the final resulting texture, but the fact remains that conventional processing of these alloys always results in a strong crystallographic texture [12]. A schematic of the TD split basal texture is shown in Figure 2.3. For thicker plates that have undergone less thickness reduction, the TD split angle may be larger, which is shown in Figure 2.4 which is a pole figure generated from an 8mm thick CP-Ti plate.

2.3 Slip transfer

During plastic deformation of a polycrystal, each grain is constrained by its neighbours. Dislocations are free to move within their grain of origin, however once they reach the grain boundary, the change in crystal orientation blocks the dislocation motion. If many dislocations pile-up at a boundary, a significant stress concentration begins to form, which also exists on the other side of the boundary. Once a certain activation threshold is met, the generation of new dislocations in the neighbouring grain at the boundary may occur as a means to alleviate the stress buildup. Similarly, the shape changes associated with the motion of these new dislocations could allow the annihilation or partial absorption of the incoming dislocation pile up. This process is known as slip

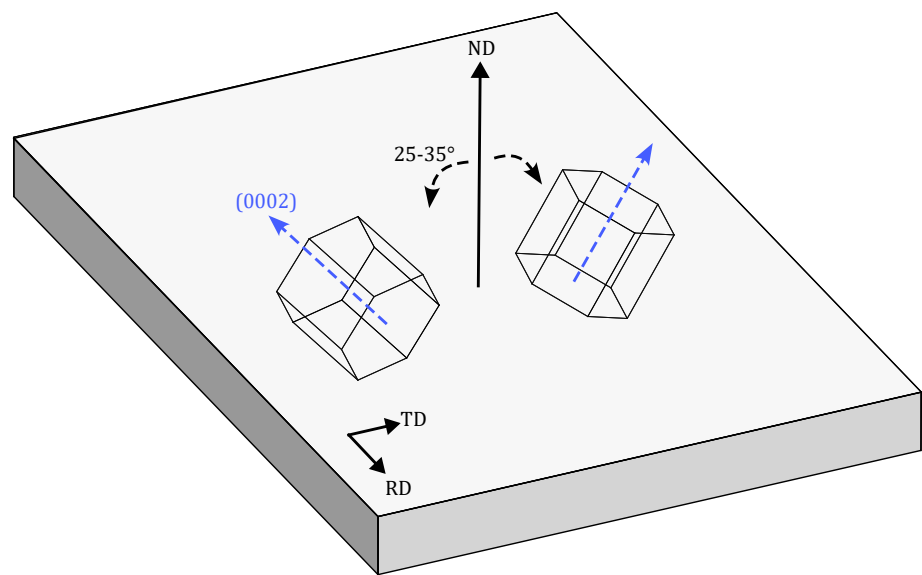


FIGURE 2.3: Schematic of the typical rolling texture for Ti/Zr: TD-split basal texture.

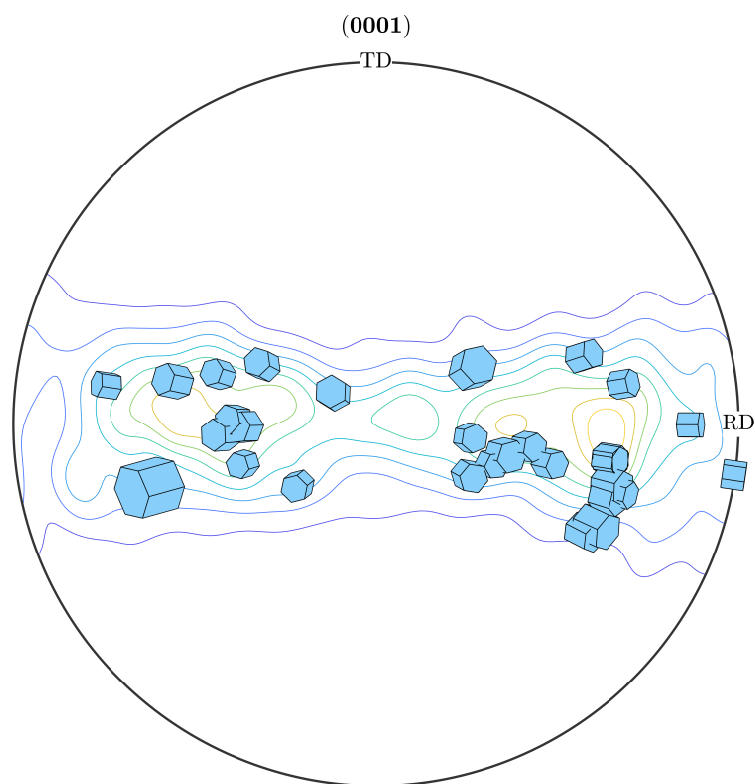


FIGURE 2.4: Pole figure of rolled CP-Ti, selected grain orientations superimposed.

transfer: incoming slip bands impinging on the grain boundary, and subsequent outgoing slip bands in an adjacent grain [13–15].

It has been well established that the geometric relationship between grains, specifically the alignment of the active incoming and outgoing slip systems, plays a major role in determining whether slip transfer occurs across a given grain boundary. The Luster-Morris parameter, m' , is a metric to quantify this geometric alignment between slip systems. It is defined as $m' = \cos(\psi) \cos(\kappa)$, where ψ is the angle between slip plane normal vectors, and κ is the angle between Burgers vectors. This parameter varies between 0 and 1, with values closer to 1 indicated good geometric alignment and high probability of slip transfer [16].

This metric can serve as the basis for understanding how grains accommodate each other, and can be extended beyond pair interactions to describe longer networks of accommodation and grain cluster effects [17].

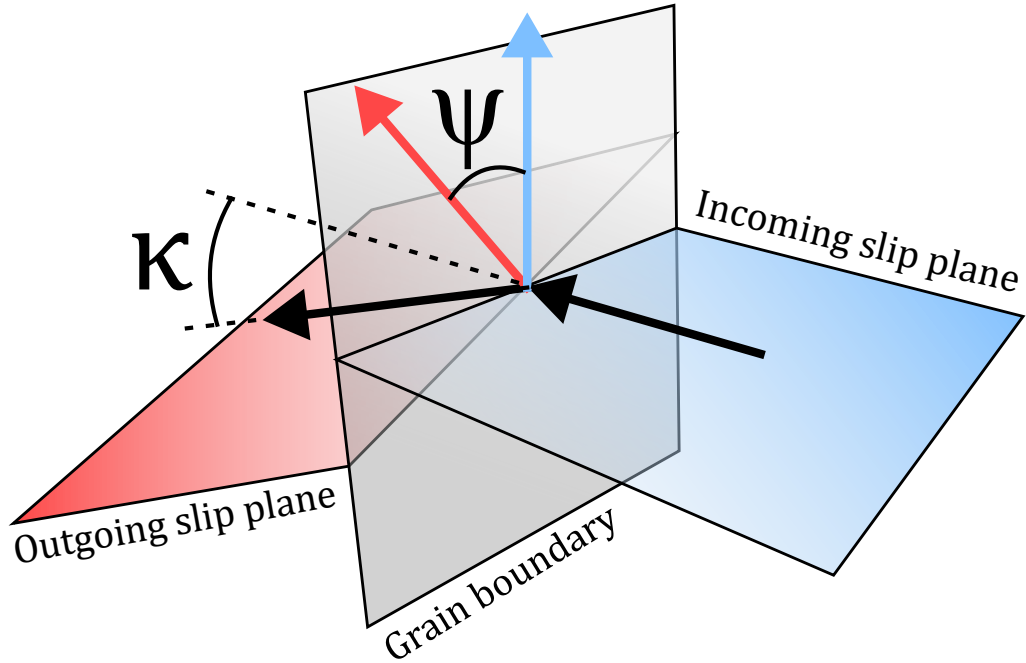


FIGURE 2.5: Geometry of slip transfer event, black arrows indicate Burgers vectors, coloured arrows indicate slip plane normal vectors.

Chapter 3

Research aims

Aims

1. Create texture-free HCP alloys (Ti/Zr) using HIP
2. Inform crystal plasticity model with mechanical testing results
3. Gain deeper understanding of fundamental deformation behaviour, especially polycrystal neighbourhood effects using in-situ methods
4. Use insights to develop novel behaviour law for crystal plasticity models

Objectives

HIP process:

- Determine working HIP parameters for producing desired material
- Consider how temperature and pressure profiles, dwell time, powder stock, can geometry, and packing density affect the final microstructure (porosity, grain size distribution)

Perform comprehensive mechanical testing:

- Generate accurate and reliable experimental data from standard mechanical tests (tensile tests, cyclic loading, hot compression)

Inform CP-FFT model:

- Create virtual representative volume element using Dream3D, use MFront to define material behaviour law, use AMITEX to solve constitutive equations in FFT regime
- Perform parameter fitting using mechanical test data
- Evaluate model generality with respect to texture by comparing results for HIPed and conventionally processed material

In-situ testing

- Use HR-DIC to track plastic strain during loading
- Employ Relative Displacement Ratio (RDR) analysis to identify active slip systems
- Correlate deformation to local grain neighbourhood

Development of novel crystal plasticity behaviour law

- Incorporate grain boundary effects such as geometric compatibility
- Utilise composite voxels to accurately describe grain boundary geometry and incorporate complex interfacial effects

Chapter 4

Methodology

4.1 Hot Isostatic Press (HIP)

In order to produce random-texture HCP metal, commercially pure titanium powder was consolidated into a bulk solid using hot isostatic pressing. Three different powder stocks were available for this project, all grade 2 titanium but with different powder particle size distributions. These size distributions were listed as $15 - 53\mu\text{m}$, $45 - 90\mu\text{m}$, and $50 - 150\mu\text{m}$. The powder was packed into a cylindrical stainless steel can, which had internal diameter of 50mm and internal height of 120mm. A bottom and a top cap were welded to the cylindrical casing, with the top tube including a small filling tube to allow insertion of the powder. The powder packing was done by hand using a funnel. Shaking and knocking the outside of the can to condense the powder resulted in a good packing density which was estimated to be 70% based on mass gain.

The can was evacuated through the filling tube at the top of the can over several hours to remove the gas between the powder particles. This filling tube was then crimped and the end of the tube was welded to ensure a complete seal. Once fully sealed, the can was placed inside the HIP chamber and the run was commenced with the following program. Importantly, the maximum temperature during this program was measured with a thermocouple to be 854°C which is below the expected β -transus of CP-Ti which is approximately 920°C . Staying below the beta transus is very important due to the vastly different grain boundary mobility between the alpha and beta phases. The BCC crystal structure of the beta phase allows for much faster grain growth, which would not be ideal for studying equiaxed polycrystalline behaviour.

HIP program:

1. Evacuate to 1 torr
2. Pump up to 100 Bar
3. Pump up to 1500 Bar & ramp up to 850°C over 170 minutes
4. Dwell for 240 minutes
5. Vent to 100 Bar and ramp down to 100°C over 150 minutes
6. Free cool to 75°C
7. Vent to 20 Bar

Because of the isostatic stress condition, it was hypothesised that no preferred crystallographic orientations would exist, and therefore no texture development would occur. The mechanisms that drive texture development during conventional processing are a response to the directionally dependent stress state, in which grains of certain orientations behave differently. During the HIP, the plasticity that powder particles experience is dependent on the local contact points of adjacent powder particles, which can be assumed to be random. These local stress conditions can also be assumed to be on average isostatic, meaning no orientation dependent phenomena should occur.

The major limitations associated with HIPing are the cost, time and the inability to monitor the microstructure at intermediate stages.

4.2 Optical microscopy

Optical microscopy using polarised light was used for routine microstructure characterisation. Sample preparation involved grinding with silicon carbide paper (800, 1200, 2500 grit) followed by chemical-mechanical polishing using a mixture of 1 part H₂O₂(30%) with 4 parts OP-S using a Struers MD-Chem polishing cloth. During the OP-S polishing step, it is important to apply pressure so that the reaction products can be mechanically removed.

The Olympus GX51 optical microscope was used for the majority of optical characterisation as it supports usage of polarising filters. The HCP material that this project deals with (CP-Ti and Zr alloys) have an interaction with polarised light that allows for crystallographic contrast. When these materials are viewed under cross polarisers, the intensity of reflected light depends on the orientation of the $\langle c \rangle$ -axis with respect to

the viewing axis. Therefore, when a polycrystal is observed, good contrast between the grains is achieved due to differences in their crystal orientation.

This technique has limited quantitative effectiveness, it cannot determine the full crystal orientation (only the $\langle c \rangle$ -axis tilt) and some other factors affect the intensity such as the surface morphology and the angle between cross polarisers.

4.3 Electron Backscatter Diffraction (EBSD)

Electron microscopy techniques can be used to acquire full quantitative information about the crystallographic orientations within samples. This project utilises the JEOL IT800 SEM equipped with an Oxford EBSD symmetry detector. EBSD is a very widespread technique among published literature as it offers high resolution imaging, phase mapping and grain identification. The procedure involves mounting a small sectioned and polished sample inside the SEM stage and tilting the stage by 70° . The EBSD detector can then be calibrated for background corrections in order to receive a high quality signal of Kikuchi bands, which are used to identify material phases and calculate the orientation. Electropolishing is necessary to obtain pristine sample surface quality before EBSD analysis if high resolution imaging is required. For texture analysis, large area and low resolution imaging is sufficient.

Some care must be taken regarding the conventions for describing HCP orientations. The Oxford convention is to report the Euler angles by the Bunge convention (as passive rotations from the sample frame to the crystal frame) and defining the local X axis as being parallel to the crystal $\langle a \rangle$ -axis.

For general characterisation, optical microscopy is preferred due to its time and cost efficiency, however EBSD was used when quantitative crystallographic orientation data was needed.

4.4 Mechanical testing

Cylindrical samples were machined with a gauge diameter of 3mm and gauge length of 15mm. Uniaxial tensile tests were conducted using screw-driven Instron testing machines with a strain rate of 0.02mm/s. The 10kN load cell was used to maximise accuracy of the force transducer measurements, since the load on the sample was expected to reach 7kN which is outside the ideal range for the 100kN load cell. An extensometer was attached to the sample for accurate strain measurements.

Circular samples are preferred because it is easier to obtain good alignment of the sample with the loading axis, which ensures accurate and reproducible data. Small sample geometry was chosen in order to maximise the number of samples that could be made from a single HIP can, since the HIP runs are costly.

4.5 Crystal plasticity modelling

The modelling strategy is to build a workflow that can be easily adapted to fit many materials problems of similar nature. The software packages that were chosen were selected to be ones that could be easily customised and compartmentalised. This basic workflow can be divided into three main stages: material, behaviour, solver.

The simulated material that will be used for the crystal plasticity model, known as the representative volume element, is a virtual reconstruction of the polycrystalline microstructure that contains all the information about the material properties and crystallographic orientations. In our case, this can be stored as a set of *.vtk* files that represent the material information as a volume of 3-dimensional elements known as voxels. The software package chosen for the generation and manipulation of these material files is Dream3D. Both synthetic material construction and experimentally informed reconstruction (using EBSD data) can be done with Dream3D.

The material behaviour laws which describe the crystal plasticity behaviour explicitly can be created and compiled into machine language with the MFront library [18]. Here the detailed interactions between different deformation modes and their hardening behaviours can be described and tweaked.

Finally, the solver that was selected is AMITEX which is an open source project that specialises in fast fourier transform (FFT) based algorithms for solving materials modelling problems. AMITEX has straightforward documentation detailing how to import materials and behaviour files, and also how to control the loading conditions of the simulation. The advantage of AMITEX is its portability and customisability, as well as some unique advanced features such as composite voxels which allow for multiple behaviour laws to operate within a single material point, allowing smooth boundaries and complex interfaces to be handled properly which is one of the major struggles previously with FFT methods.

Chapter 5

Research completed to date

5.1 CP-Ti plate

Conventionally processed CP-Ti (grade 2) plate with a thickness of 8mm, and sheet with a thickness of 0.7mm, were purchased from Specialty Metals. Both the plate and sheet had undergone a recrystallisation anneal but the exact process parameters were not reported. Optical microscopy was used for basic microstructure characterisation, shown in Figure 5.1, and found equiaxed α -Ti grains. The average grain size (linear intercept) for the plate and sheet were 25 μm and 15 μm respectively.

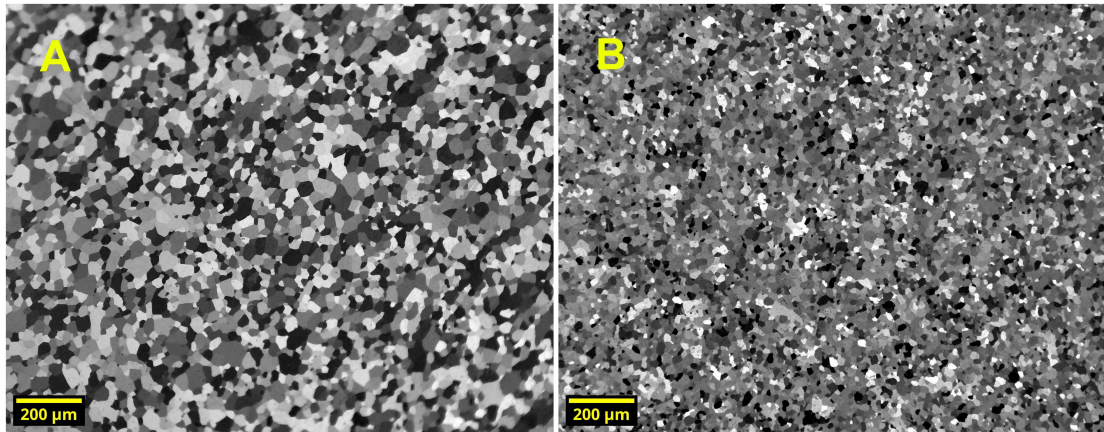


FIGURE 5.1: Polarised light optical micrograph of CP-Ti plate (A) and sheet (B).

Crystallographic texture measured with EBSD revealed a strong split basal texture in the CP-Ti plate, with a large TD split angle of approximately 45°, as shown in Figure 5.2. The large TD split is interesting because it exaggerates the already present anisotropy that is typical with a less pronounced TD split basal texture, with many grains having components of their $\langle c \rangle$ -axis along TD but almost zero grains having $\langle c \rangle$ -axis components along RD.

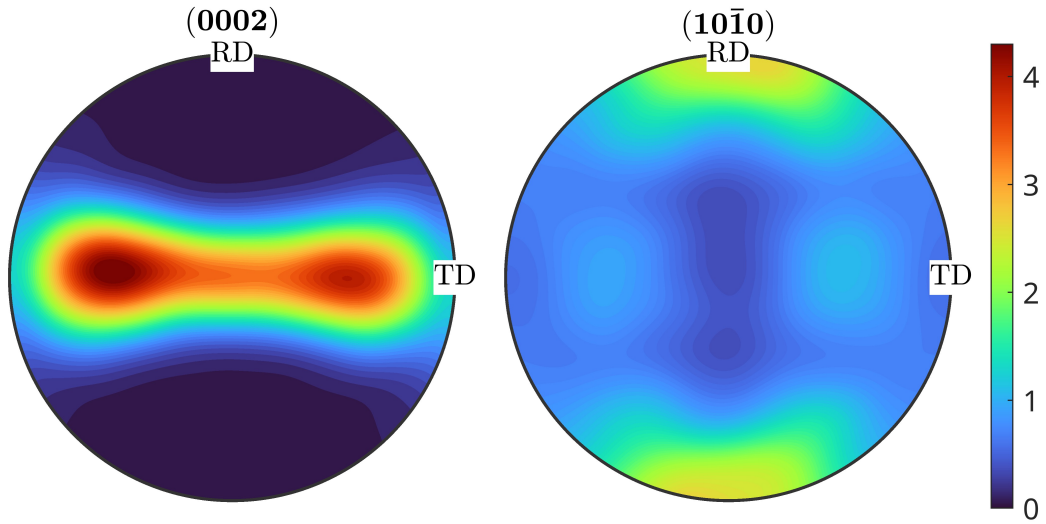


FIGURE 5.2: Pole figures for CP-Ti plate, colour scale indicates multiples of random distribution.

To examine the effect of such a strong texture, cylindrical samples along RD and TD were fabricated for tensile testing. The results of tensile testing, shown in Figure 5.3, reveal the significant anisotropy in mechanical response between the two primary plate directions. The yield behaviour was completely different between both samples, with the RD sample undergoing a much earlier and smoother elastic-to-plastic transition. For TD loading on the other hand, a much higher yield followed by a yield plateau was observed.

To quantify the early plasticity observed in the RD sample, the point where the stress-strain curves of the two samples diverge was determined. The elastic limit was defined as the point when measurable plasticity in the RD sample had occurred. The stress-strain data for both RD and TD was interpolated so that their stress difference at each strain point could be calculated by subtraction. This difference function is plotted in Figure 5.4. During the elastic region, both samples behave very similarly and the difference remains flat. This region was classified as the first 0.08% strain, and the mean and standard deviation of the difference was determined. Measurable plasticity was defined to be the point where the RD sample had deviated by more than 2 times the standard deviation, which occurred at a strain of 0.1% and a stress of 111MPa.

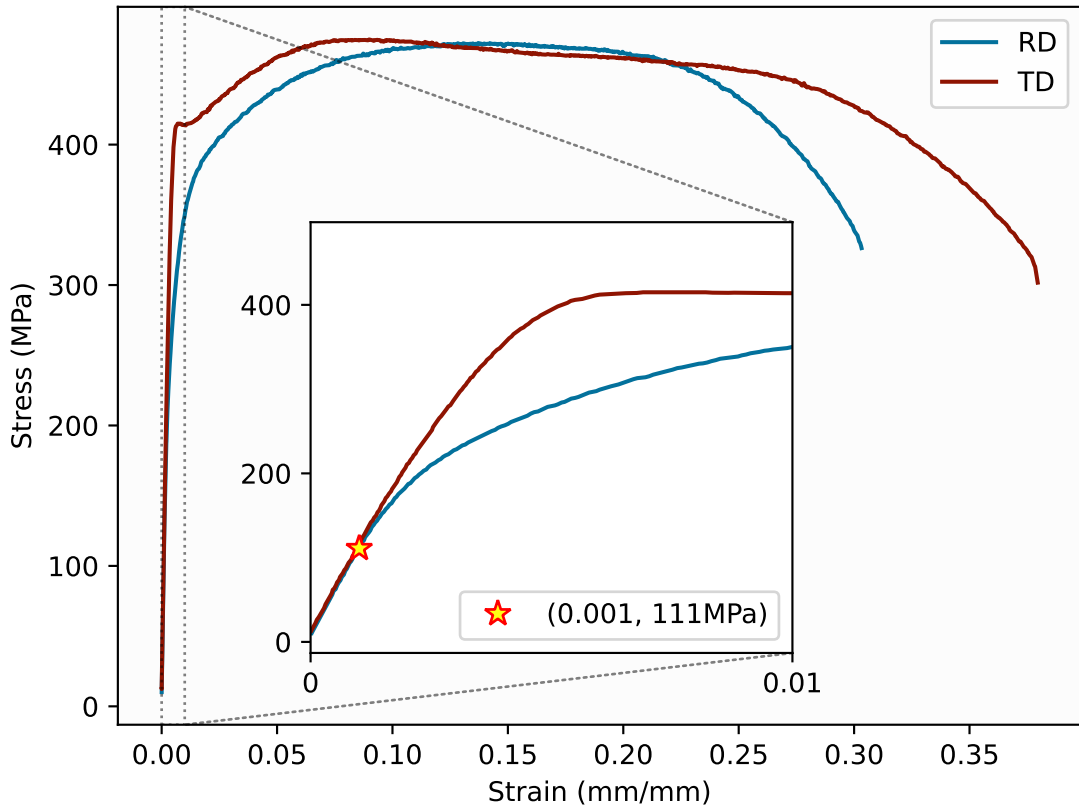


FIGURE 5.3: Engineering stress-strain curve for CP-Ti for both rolling direction (RD) and transverse direction (TD). Elastic limit of RD sample marked on inset plot.

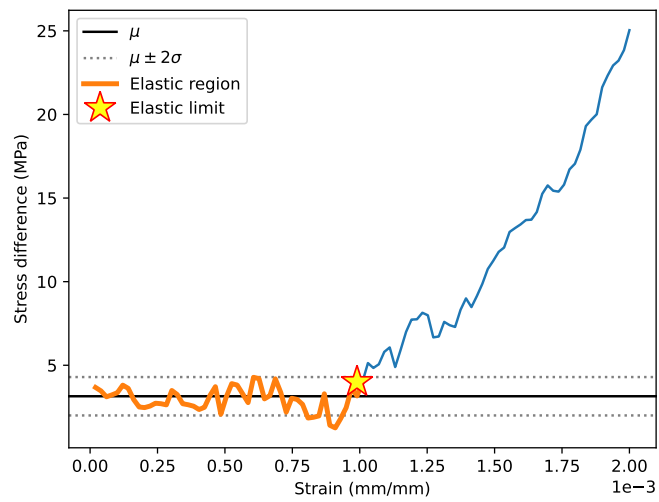


FIGURE 5.4: Stress difference ($\sigma_{TD} - \sigma_{RD}$) as a function of strain, revealing when the deformation behaviour diverges, indicating elastic limit of RD.

5.2 HIP #1: Abnormal grain growth

The first HIP run appeared successful, and initial characterisation with EBSD revealed the desired microstructure of equiaxed α grains. This initial characterisation however, was only conducted on a small part of the bottom of the HIP can. Subsequent tensile testing results are shown in Figure 5.5, in which strange load drop behaviour can be observed. These load drops were accompanied by audible pings and were present in all 5 samples that were cut from the initial HIP can. After some difficulty in explaining this phenomenon with respect to the assumed equiaxed microstructure, further characterisation of the material was made using cutoffs from the head sections of the tensile samples.

These cutoffs were etched using Kroll's reagent (1% HF + 4% HNO₃ + 95% H₂O) and it was discovered that significant abnormal grain growth had occurred during the HIP, shown in Figure 5.6. Very large grains can be seen which have grown to sizes on the order of several millimetres. These grains appear to exist within a surviving matrix of normal grains which appear to be the same as the initially observed section of the HIP can, which did not present any abnormal grains.

The precise mechanism for the abnormal grain growth is not known. It is known in the literature that the recrystallisation behaviour of alpha titanium is quite sensitive when held at high temperatures (but still beneath the beta-transus)[19]. Usually this phenomenon is related to recrystallisation after small strains, where the number density of recrystallisation nuclei may be quite small. In such a regime, once recrystallisation nucleates, the new grain has unimpeded growth. Provided that the small amount of work stored in the matrix is sufficient to support its growth, the new grain may grow to a very large size if there were no nearby recrystallisation nuclei. The small strain in our case would be the initial plasticity required for consolidation of the powder.

In order to gain a deeper understanding and also as a second attempt at producing a fully random texture and consolidated HCP material, a second HIP was run using the two alternative powder stocks. There was evidence of powder contamination in the original material, and therefore it was a plausible option to retry the same parameters with a different and hopefully uncontaminated powder. The difference in powder size distribution would also change the dynamics of the early stage plasticity during consolidation and hopefully lead to a different result.

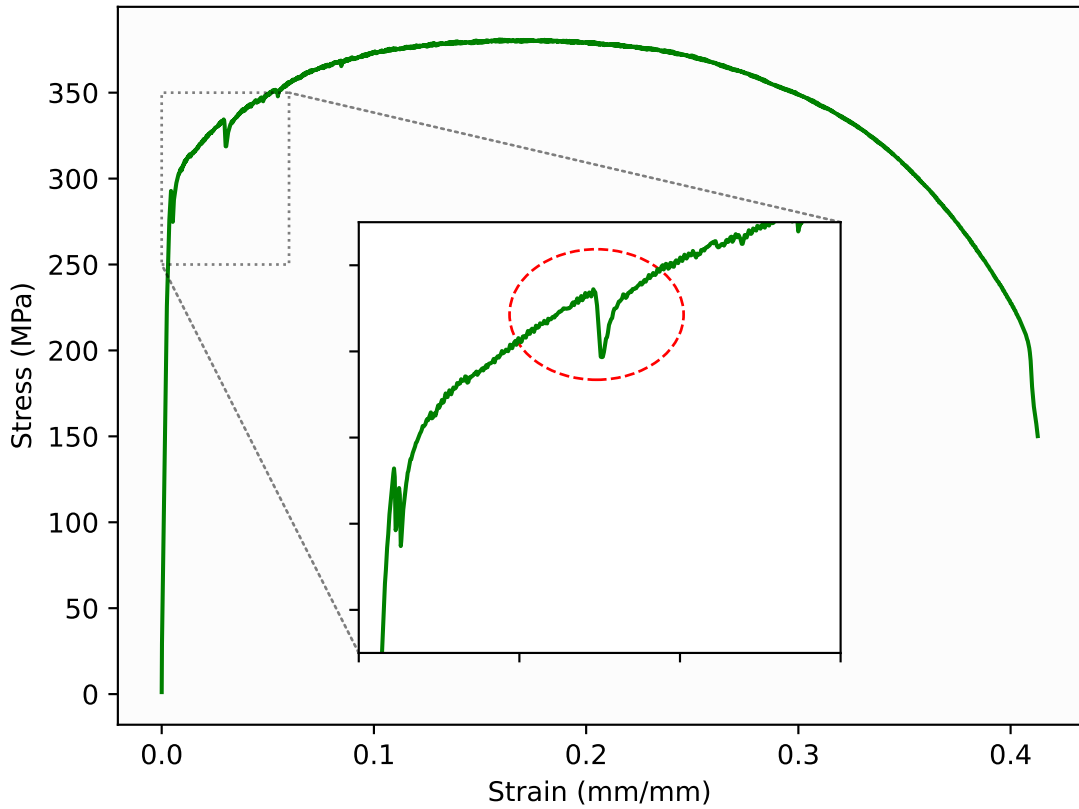


FIGURE 5.5: Engineering stress-strain curve for HIP CP-Ti. Later discovered abnormal grain growth to be the cause of load drops.



FIGURE 5.6: Optical micrograph of HIPed CP-Ti abnormal grain growth with Kroll's etch.

5.3 HIP #2: Success

The second HIP trial was indeed successful, in both cases. The two powder stocks that were used were the 45-90 μm (TLS powder) and the 53-100 μm (AVI powder). The resulting microstructure these cans had a grain size distribution of approximately 50 μm and 60 μm respectively (which may indicate that powder particle size is well correlated to final grain size).

The texture of the second HIP was quantified using EBSD large area measurements, which sampled many grains to generate pole figures, shown in Figure 5.7. The same

colour scale from Figure 5.2 which highlights the sharp difference in texture strength. Despite lacking any distinct texture features, the pole figure is not completely flat, which can be attributed to the sampling of a limited (though large) set of grains.

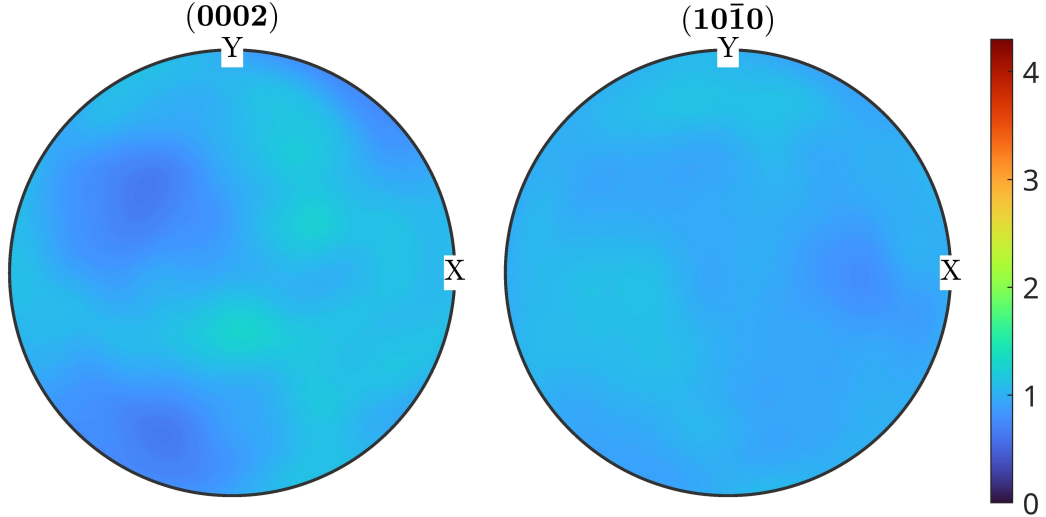


FIGURE 5.7: Pole figures for HIPed CP-Ti using same colour scale as Figure 5.2.

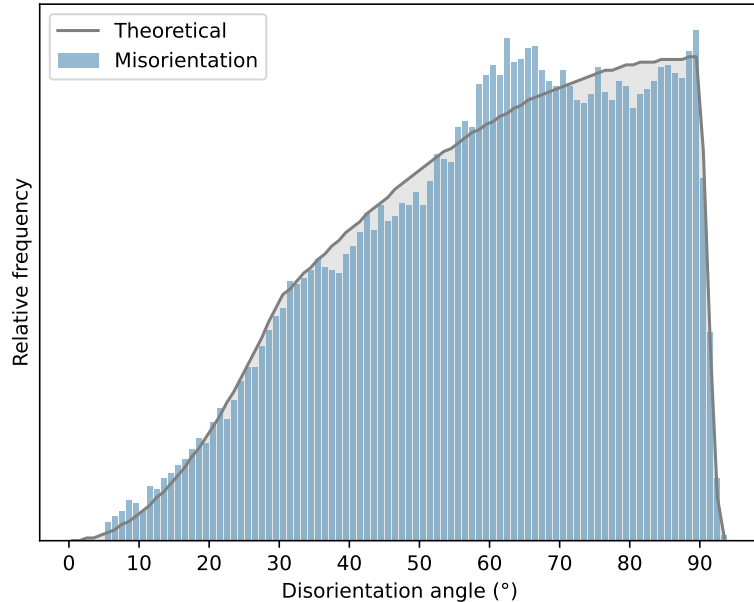


FIGURE 5.8: Disorientation distribution for HIP#2, agreement with theoretical distribution for random texture.

The random-texture can further be quantified using the three Kearns factors: 0.3363, 0.3249, 0.3388. For a theoretically random texture, the Kearns factors are each exactly 1/3. Finally, the disorientation plot in Figure 5.8 shows a very close agreement to the theoretical Mackenzie plot for a truly random orientation distribution. It is therefore concluded that HIPing has proved a successful technique for producing randomly textured HCP microstructures.

5.3.1 Geometric compatibility

EBSD maps were used to calculate the grain neighbour compatibility in both the HIPed material and the conventionally rolled material. First, a global loading condition along RD was assumed, which allowed Schmid factor analysis to be used to determine the active slip system in each grain. Only prismatic slip systems were considered for this preliminary analysis. Once the active slip systems were identified, for each neighbouring pair, the Luster-Morris parameter m' was calculated across their boundary to determine how well the pair can accommodate slip between them. A map of these m' values in the HIP material is shown in Figure 5.9, where brighter colours represent boundaries most likely to be sites for slip transfer events.

A statistical representation of the m' values is shown by the histogram in Figure 5.10. A distinct peak at the high end of m' values is present in the rolled material which is completely absent in the HIPed material. A typical threshold for direct slip transfer is $m' > 0.8$ [20]. In the rolled sample, 19% of grain boundaries are above this threshold, compared to only 7% in the HIPed sample. There is a measurable difference in the geometric alignment of neighbouring grains, which can be explained by the rolled texture having a more restricted set of possible grain orientations due to many orientations being absent from the orientation distribution (e.g. almost zero grains with c-axis aligned with RD). This means that grains are more likely to have similar orientations with their neighbours and this is reflected in the peak at higher m' values.

If polycrystalline strain localisation can be considered as a networking phenomenon, then a description based on percolation theory may be suitable. The extent of networks of geometrically aligned grains would then be dependent on the expected fraction of neighbouring grains that have good alignment.

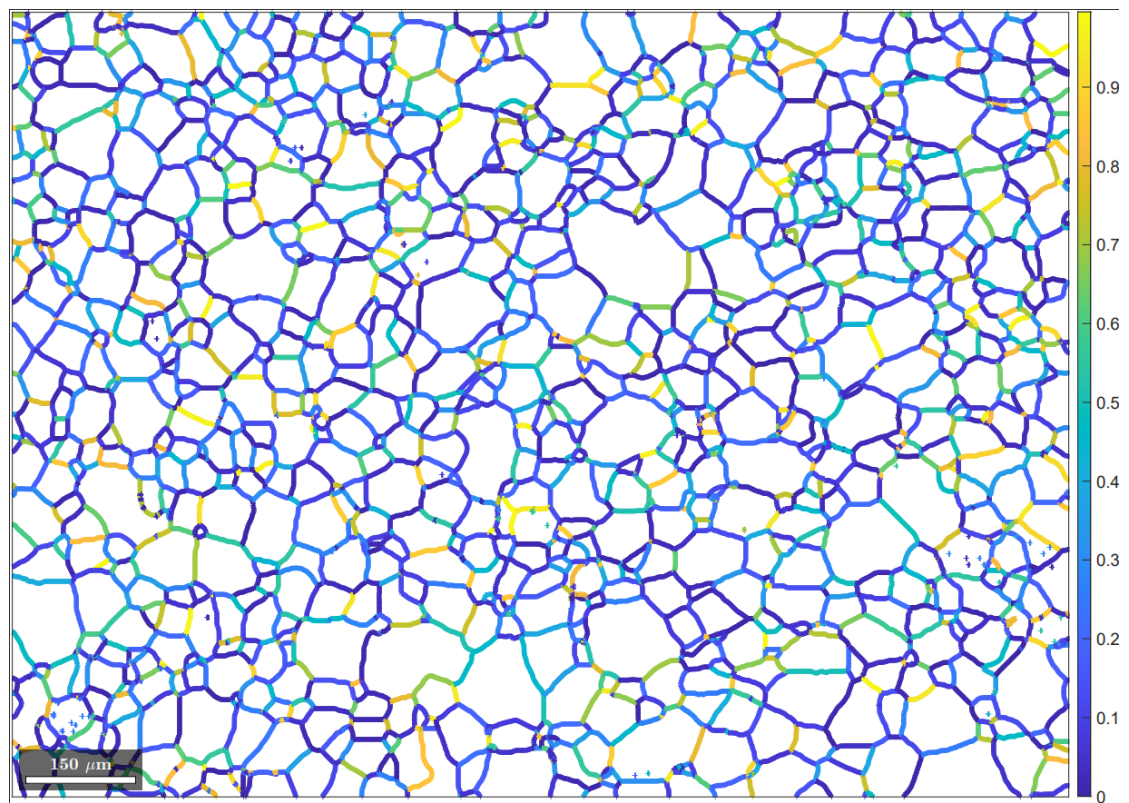


FIGURE 5.9: Map of m' values in HIPed CP-Ti.

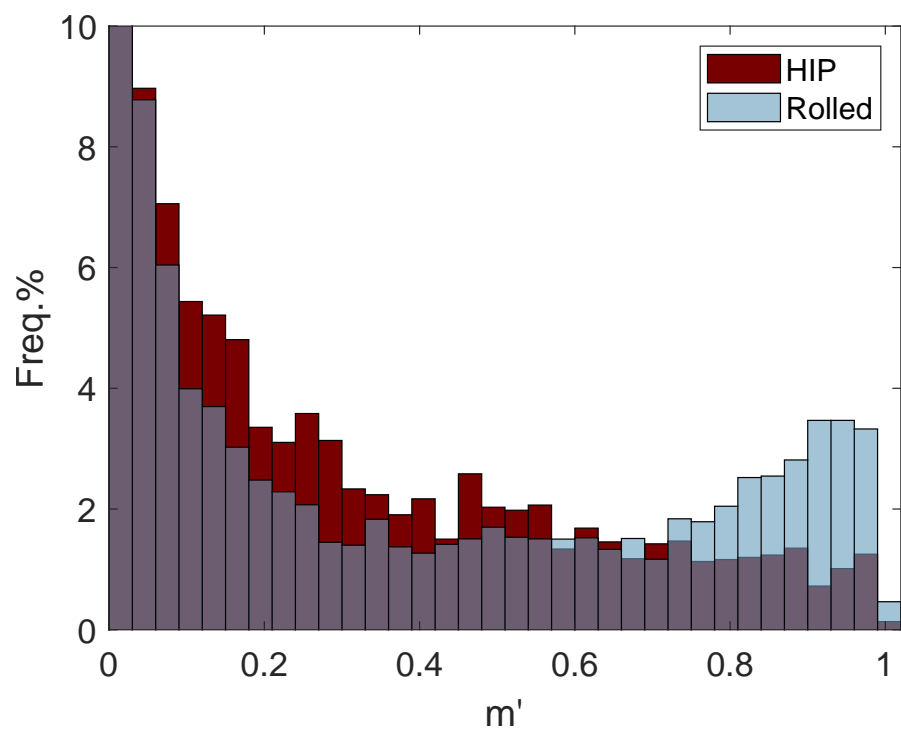


FIGURE 5.10: Histogram of m' values for rolled (RD loading) and HIPed CP-Ti.

Chapter 6

Proposed research

6.1 Mechanical testing of HIPed material

The most immediate next step in the project is the mechanical testing of the HIPed material. Simple tensile tests using the same parameters as for the rolled plate samples, and using the same sample geometry. In addition to simple uniaxial tensile testing, cycle loading tests alongside the rolled samples would allow for a comparison of the kinematic hardening behaviour between the two samples. Post-mortem analysis of the microstructure after interrupted tensile tests would also provide insight into the role that deformation twinning plays during plasticity.

6.2 HR-DIC in-situ testing

Use of the new capability at Monash Centre for Electron Microscopy (MCEM) for in-situ tensile testing would allow for high resolution digital image correlation to be used to map the strain localisation throughout the microstructure as a function of total strain. This technique, when paired with Relative Displacement Ratio (RDR) analysis would allow for identification of active slip modes and in-situ EBSD correlation would track the twinning behaviour as well as localised crystal rotation.

6.3 Rolling HIPed material

Direct comparison of the HIPed material to the purchased rolled plate is difficult as the exact alloy composition is not consistent, particularly the oxygen content, which has a significant effect on the mechanical properties. To truly isolate crystallographic texture

as the only independent variable, the HIPed material will be rolled to produce intermediate textures. This will involve rolling to multiple different thickness reductions, and then calibrating a heat treatment regime for each of them to produce a recrystallised microstructure with constant grain size across all samples. Mechanical testing and analysis of these samples would then truly highlight the transition between completely random texture to the presence of a strong crystallographic texture which is more akin to what is typically found in service.

6.4 Crystal plasticity modelling

The next stages in crystal plasticity modelling will be calibrating a twinning model to reproduce the anisotropic response from the rolled plate samples. Once tensile data for the HIPed material is obtained, it can be incorporated into the fitting regime as an additional constraint.

Beyond this, novel constitutive behaviour laws will be developed to incorporate a description of the geometric compatibility effect, especially in relation to long range networks of strain. To account for complex interfacial interactions, composite voxels will be incorporated using AMITEX.

Chapter 7

Research communication

As one of the initial nuclear research projects related to AUKUS in Australia, we plan to incorporate significant collaboration between the relevant existing international research and industrial communities. Firstly, Rolls-Royce Submarine have agreed to join the project with a co-supervisor role, which will include routine scheduled progress update meetings as well as additional direction and expertise from industry experts in nuclear submarine materials. As part of this partnership, I will spend 3 months in Manchester to integrate with the rich Zirconium community already there and to learn and develop skills that can be brought back to the Australian research community. The findings of this project are directly relevant to nuclear submarine industry and will be communicated to both Rolls-Royce Submarines and relevant Australian bodies that become involved, such as the Australian Submarine Association (ASA). It will likely be necessary to follow strict intellectual property laws since the project is related to national defence. Most of the research output of this project however will be considered 'fundamental research' which can be published in the standard scientific journals as standard academic work.

Bibliography

- [1] G. Lütjering and J.C. Williams. *Titanium*. Engineering materials and processes. Springer Berlin Heidelberg, 2013. ISBN 978-3-540-71398-2. URL <https://books.google.com.au/books?id=wBXsCAAAQBAJ>.
- [2] Christoph. Leyens, Manfred. Peters, J. Kumpfert, and ProQuest (Firm). *Titanium and Titanium Alloys : Fundamentals and Applications*. John Wiley & Sons, Incorporated, Hoboken, 1st ed. edition, 2003. ISBN 978-3-527-60520-0.
- [3] Committee B10. *Deformation Mechanisms, Texture, and Anisotropy in Zirconium and Zircaloy*. ASTM International, 100 Barr Harbor Drive, PO Box C700, West Conshohocken, PA 19428-2959, 1988. ISBN 978-0-8031-0958-2. doi: 10.1520/STP966-EB.
- [4] Michael Battaini. *Deformation behaviour and twinning mechanisms of commercially pure titanium alloys*. PhD thesis, January 2017. URL https://bridges.monash.edu/articles/thesis/DeformationBehaviour_and_twinning_mechanisms_of_commercially_pure_titanium_alloys/4534439.
- [5] L. Wang, Z. Zheng, H. Phukan, P. Kenesei, J.-S. Park, J. Lind, R.M. Suter, and T.R. Bieler. Direct measurement of critical resolved shear stress of prismatic and basal slip in polycrystalline Ti using high energy X-ray diffraction microscopy. *Acta Materialia*, 132:598–610, June 2017. ISSN 1359-6454. doi: 10.1016/j.actamat.2017.05.015. URL <https://www.sciencedirect.com/science/article/pii/S1359645417303920>.
- [6] Laura Nervo, Andrew King, Arnas Fitzner, Wolfgang Ludwig, and Michael Preuss. A study of deformation twinning in a titanium alloy by X-ray diffraction contrast tomography. *Acta Materialia*, 105:417–428, February 2016. ISSN 1359-6454. doi: 10.1016/j.actamat.2015.12.032. URL <https://www.sciencedirect.com/science/article/pii/S1359645415301385>.

- [7] J.W. Christian and S. Mahajan. *Deformation twinning*, volume 39. January 1995. URL <https://www.sciencedirect.com/science/article/pii/0079642594000077>.
- [8] H. P. Lee, C. Esling, and H. J. Bunge. Development of the Rolling Texture in Titanium. *Texture, Stress, and Microstructure*, 7(4):562818, January 1988. ISSN 1687-5397. doi: 10.1155/TSM.7.317. URL <https://doi.org/10.1155/TSM.7.317>. Publisher: John Wiley & Sons, Ltd.
- [9] Nathalie Bozzolo, Lisa Chan, and Anthony D Rollett. Misorientations induced by deformation twinning in titanium. *Journal of applied crystallography.*, 43(3): 596–602, 2010. ISSN 0021-8898. doi: 10.1107/S0021889810008228. Place: Oxford, England : Publisher: Blackwell Pub. on behalf of the International Union of Crystallography.
- [10] Yong Zhong, Fuxing Yin, and Kotobu Nagai. Role of deformation twin on texture evolution in cold-rolled commercial-purity Ti. *Journal of Materials Research*, 23(11):2954–2966, 2008. ISSN 0884-2914. doi: 10.1557/JMR.2008.0354. URL <https://www.cambridge.org/core/product/COD2489CB70055CF310545D97A0B5AB0>. Edition: 2011/01/31 Publisher: Cambridge University Press.
- [11] Wenbin Guo, Geping Li, Fusen Yuan, Fuzhou Han, Yingdong Zhang, Muhammad Ali, Jie Ren, and Gaihuan Yuan. Texture development and mechanical behavior of Zircaloy-4 alloy plates fabricated by cold rolling and annealing. *Materials Science and Engineering: A*, 807:140846, March 2021. ISSN 0921-5093. doi: 10.1016/j.msea.2021.140846. URL <https://www.sciencedirect.com/science/article/pii/S0921509321001155>.
- [12] Y.B. Chun, S.H. Yu, S.L. Semiatin, and S.K. Hwang. Effect of deformation twinning on microstructure and texture evolution during cold rolling of CP-titanium. *Materials Science and Engineering: A*, 398(1):209–219, May 2005. ISSN 0921-5093. doi: 10.1016/j.msea.2005.03.019. URL <https://www.sciencedirect.com/science/article/pii/S0921509305002376>.
- [13] Songyang Han and Martin A. Crimp. ECCI analysis of shear accommodations at grain boundaries in commercially pure alpha titanium. *International Journal of Plasticity*, 131:102731, August 2020. ISSN 0749-6419. doi: 10.1016/j.ijplas.2020.102731. URL <https://www.sciencedirect.com/science/article/pii/S0749641919307685>.
- [14] B. Cui, J. Kacher, M. McMurtrey, G. Was, and I.M. Robertson. Influence of irradiation damage on slip transfer across grain boundaries. *Acta Materialia*, 65:

- 150–160, February 2014. ISSN 1359-6454. doi: 10.1016/j.actamat.2013.11.033. URL <https://www.sciencedirect.com/science/article/pii/S1359645413008835>.
- [15] Y. Guo, D.M. Collins, E. Tarleton, F. Hofmann, J. Tischler, W. Liu, R. Xu, A.J. Wilkinson, and T.B. Britton. Measurements of stress fields near a grain boundary: Exploring blocked arrays of dislocations in 3D. *Acta Materialia*, 96:229–236, September 2015. ISSN 1359-6454. doi: 10.1016/j.actamat.2015.05.041. URL <https://www.sciencedirect.com/science/article/pii/S1359645415003626>.
- [16] Eugenia Nieto-Valeiras, Eshan Ganju, Nikhilesh Chawla, and Javier LLorca. Assessment of slip transfer criteria for prismatic-to-prismatic slip in pure Ti from 3D grain boundary data. *Acta Materialia*, 262:119424, January 2024. ISSN 1359-6454. doi: 10.1016/j.actamat.2023.119424. URL <https://www.sciencedirect.com/science/article/pii/S1359645423007541>.
- [17] Hamidreza Abdolvand, Jonathan Wright, and Angus J. Wilkinson. Strong grain neighbour effects in polycrystals. *Nature Communications*, 9(1):171, January 2018. ISSN 2041-1723. doi: 10.1038/s41467-017-02213-9. URL <https://doi.org/10.1038/s41467-017-02213-9>.
- [18] Thomas Helfer, Bruno Michel, Jean-Michel Proix, Maxime Salvo, Jérôme Sercombe, and Michel Casella. Introducing the open-source mfront code generator: Application to mechanical behaviours and material knowledge management within the PLEIADES fuel element modelling platform. *Computers & Mathematics with Applications*, 70(5):994–1023, September 2015. ISSN 0898-1221. doi: 10.1016/j.camwa.2015.06.027. URL <https://www.sciencedirect.com/science/article/pii/S0898122115003132>.
- [19] Vivian S. Tong and T. Ben Britton. Formation of very large ‘blocky alpha’ grains in Zircaloy-4. *Acta Materialia*, 129:510–520, May 2017. ISSN 1359-6454. doi: 10.1016/j.actamat.2017.03.002. URL <https://www.sciencedirect.com/science/article/pii/S1359645417301817>.
- [20] E. Nieto-Valeiras, A. Orozco-Caballero, M. Sarebanzadeh, J. Sun, and J. LLorca. Analysis of slip transfer across grain boundaries in Ti via diffraction contrast tomography and high-resolution digital image correlation: When the geometrical criteria are not sufficient. *International Journal of Plasticity*, page 103941, March 2024. ISSN 0749-6419. doi: 10.1016/j.ijplas.2024.103941. URL <https://www.sciencedirect.com/science/article/pii/S0749641924000688>.